Electronic Supplementary Information for

Surface Enriching Promotes Decomposition of Benzene from Air

Tao Luo,[a,b] Zhijian Wang,[b] Xuhui Wei,[b] Xiang Huang,[*c] Shuli Bai[*a] and Jiazang Chen[*b]

[a]School of Biotechnology and Health Sciences, Wuyi University, Jiangmen 529020, China

[b]State Key Laboratory of Coal Conversion, Institute of Coal Chemistry, Chinese Academy of Sciences, Taiyuan 030001, China

[c]Department of Physics, Southern University of Science and Technology, Shenzhen 518055, China

[*]Author to whom correspondence should be addressed.

Email: chenjiazang@sxicc.ac.cn (J.C.); baibsli@126.com (S.B.); huangx8@sustech.edu.cn (X.H.)

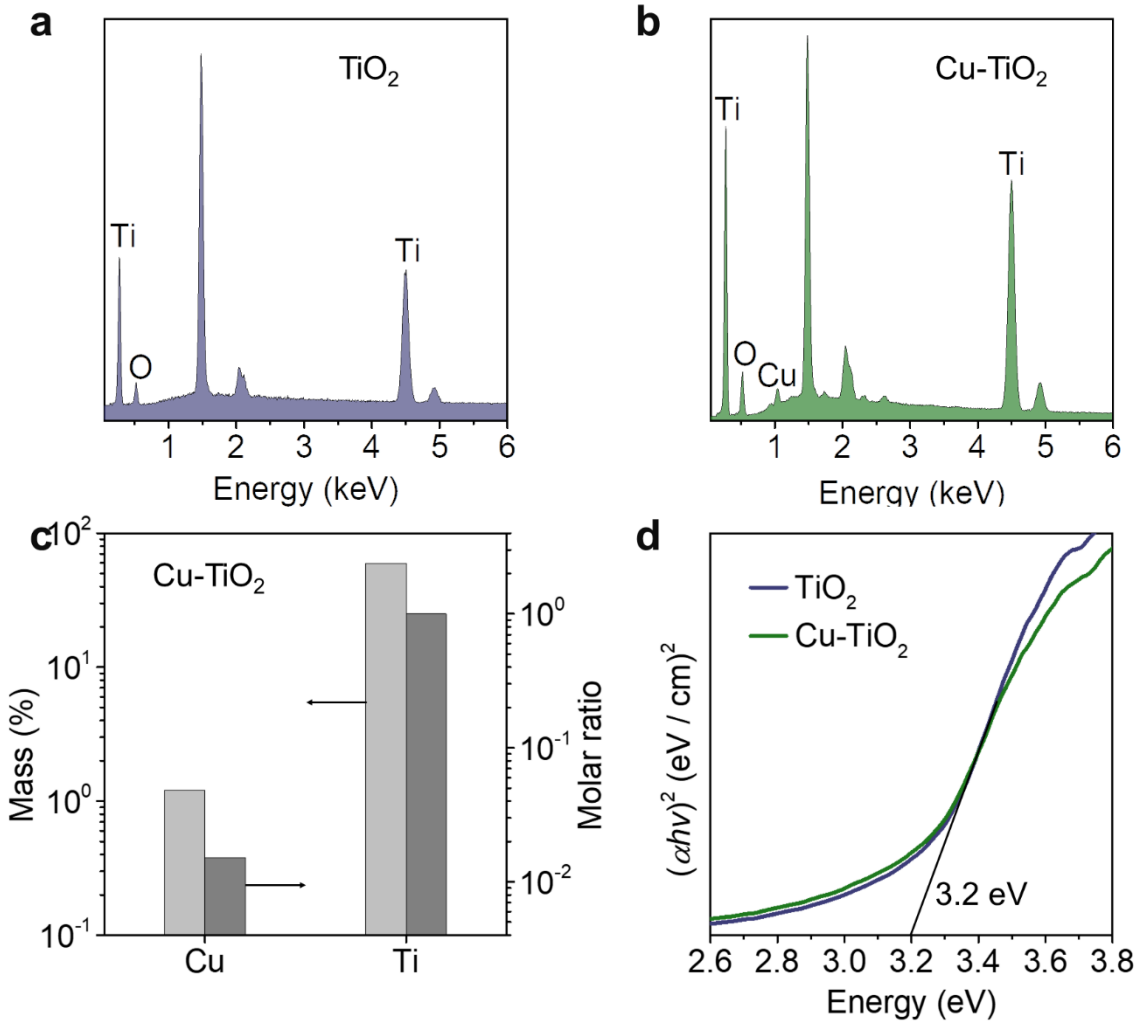

Figure S1. Energy dispersive X-ray spectroscopy results (a, TiO_2; b, Cu-TiO_2) display the signal of copper for the sample prepared with addition of $Cu(NO_3)_2$. The elemental analysis characterized by inductively coupled plasma shows that the weight proportions of Cu and Ti in the Cu-TiO_2 sample are 1.208 and 59.664 %, respectively (c). The calculated ratio of Cu to Ti is 0.0152: 1 (c). By drawing the tangent line to the Tauc plots of TiO_2 and Cu-TiO_2, it shows that doping TiO_2 with copper does not change the bandgap (d).

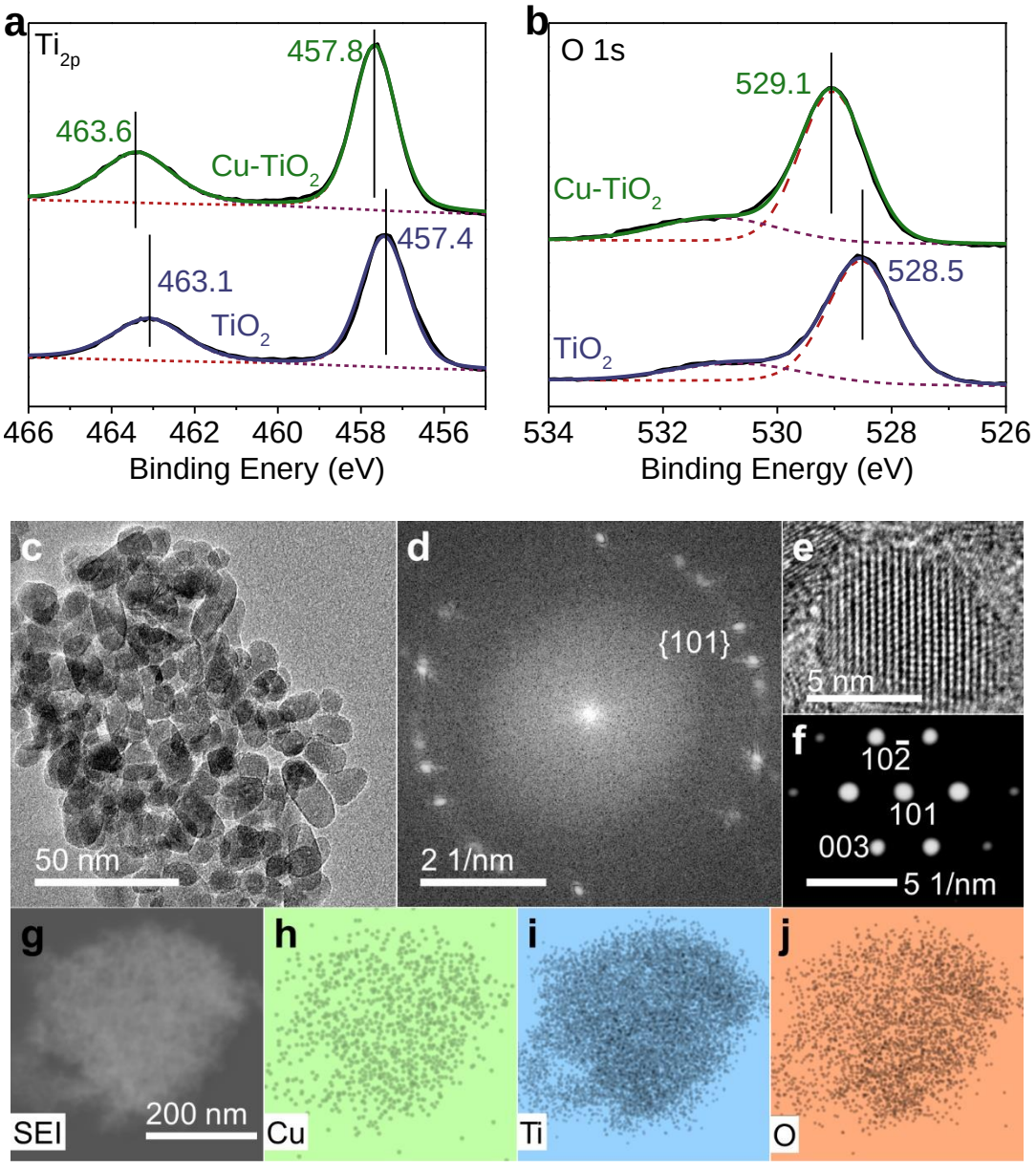

Figure S2. XPS patterns show that the $Ti_{2p3/2}$ and $Ti_{2p1/2}$ peaks slightly shift to higher binding energy after copper doping (a). These phenomena are very similar to the situation of O_{1s}, the binding energy for the lattice oxygen for the Cu-TiO_2 is ~0.6 eV higher than that of TiO_2 (b). Transmission electron microscopy (TEM) image (c) and the related selected electron diffraction pattern (SAED, d) show that Cu-TiO_2 is of ~20 nm in average diameter and phase-pure anatase. The high-resolution TEM image (e) and the SAED show that the particles is of single-crystalline anatase (f). The elemental mappings (h-j) match the electron microscopy image (g). This information indicates that the copper dopant is of uniform distribution in the Cu-TiO_2 (g-j).

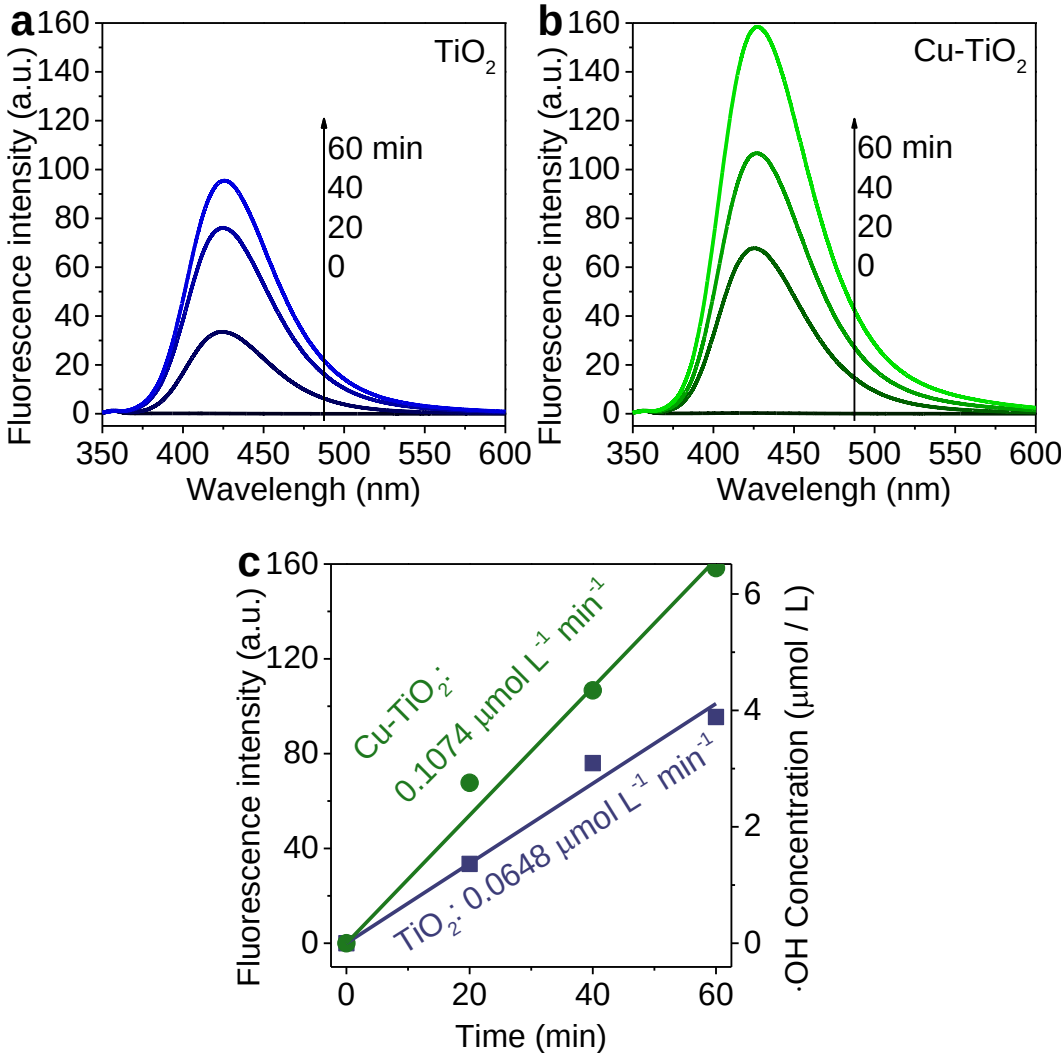

Figure S3. The photo-induced behaviors of TiO_2 (a) and Cu-TiO_2 (b) for generation of hydroxyl radicals. The concentration of hydroxyl radicals determined by photoluminescence spectroscopy shows that generation rates are 0.0648 and 0.1074 mol L^{-1} min^{-1} respectively for TiO_2 and Cu-TiO_2 (c).

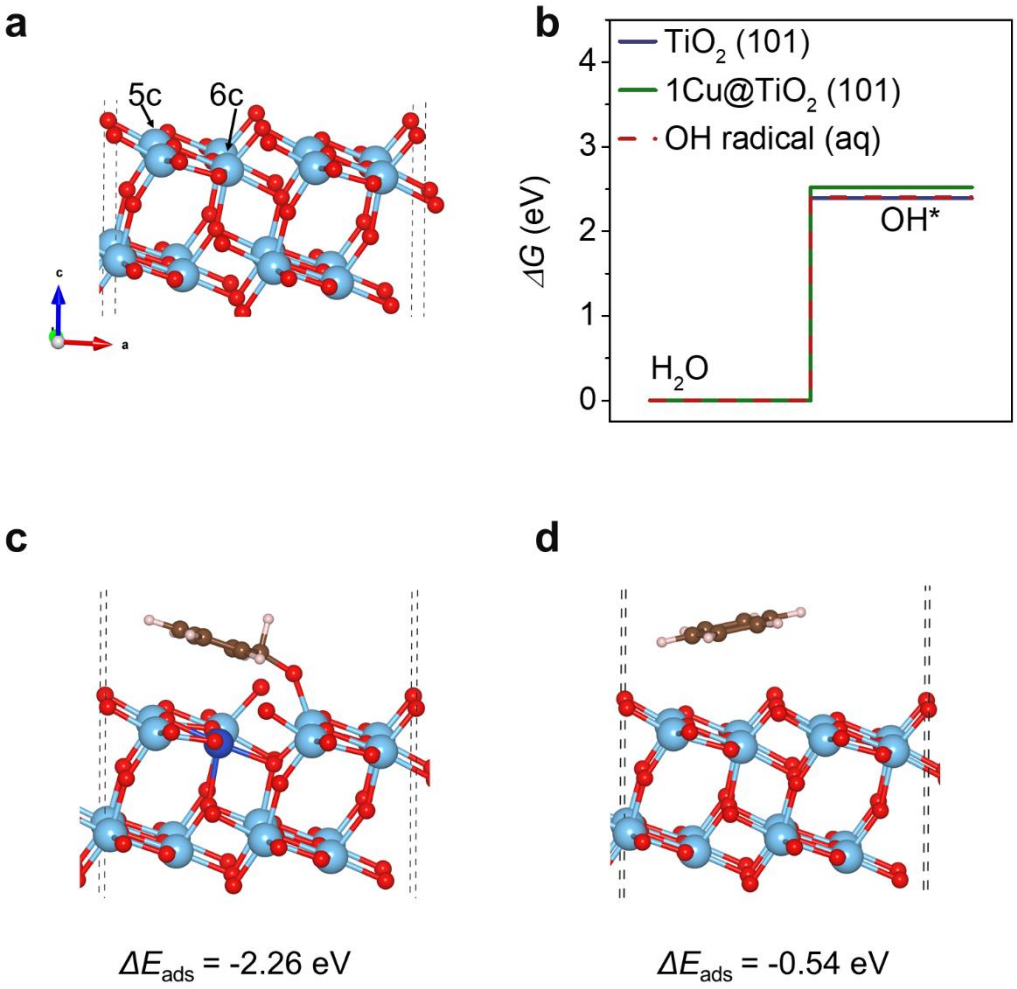

Figure S4. Density functional theory calculations for the ·OH radical production and benzene adsorption on the anatase (copper-doped) TiO_2 (101) surface. For the case of Cu-TiO_2, the 6c-Ti on the surface is substituted by a Cu atom, and a 5c-Ti is chosen as the active site for the H_2O oxidation (a). The calculated adsorption free energy of OH^* (ΔG_{OH*}) on 1Cu@TiO_2(101) is 2.52 eV, which is 0.12 eV larger than that on perfect TiO_2(101) (b). The benzene chemisorbs on 1Cu@TiO_2(101) via bonding with a bridge oxygen atom with an adsorption energy of -2.26 eV (c). The adsorption of benzene on TiO_2(101) is dominated by the Van der Waals interaction, with an adsorption energy of -0.54 eV (d).

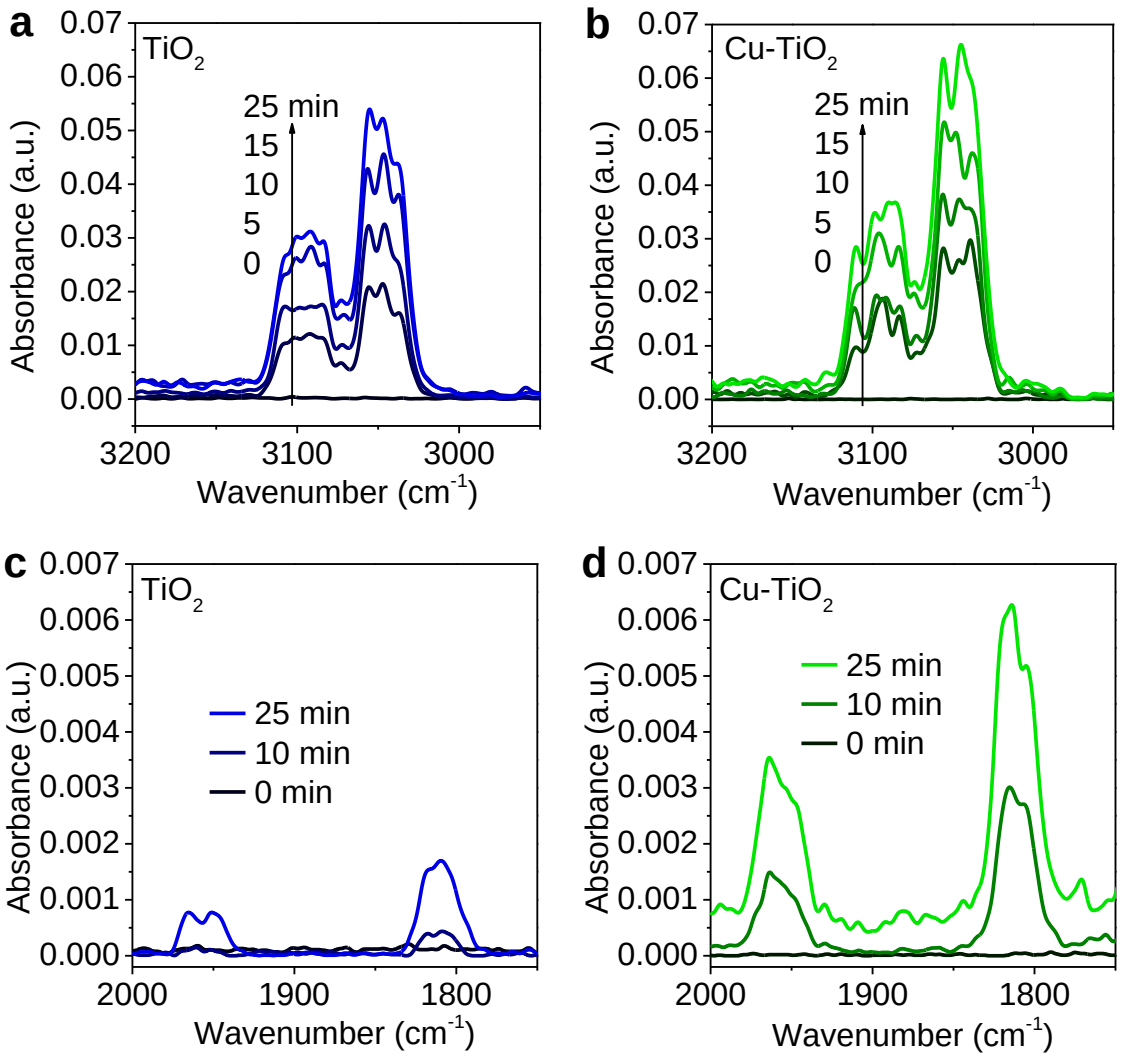

Figure S5. The absorption behaviors of benzene by TiO_2 (a, c) and Cu-TiO_2 (b, d) determined by *in situ* diffuse reflectance infrared Fourier transform spectroscopy (DRIFT).

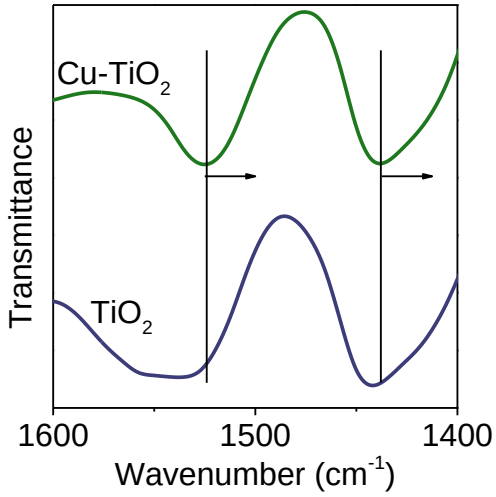

Figure S6. The redshift of characteristic peaks of benzene absorbed by TiO_2 and Cu-TiO_2.

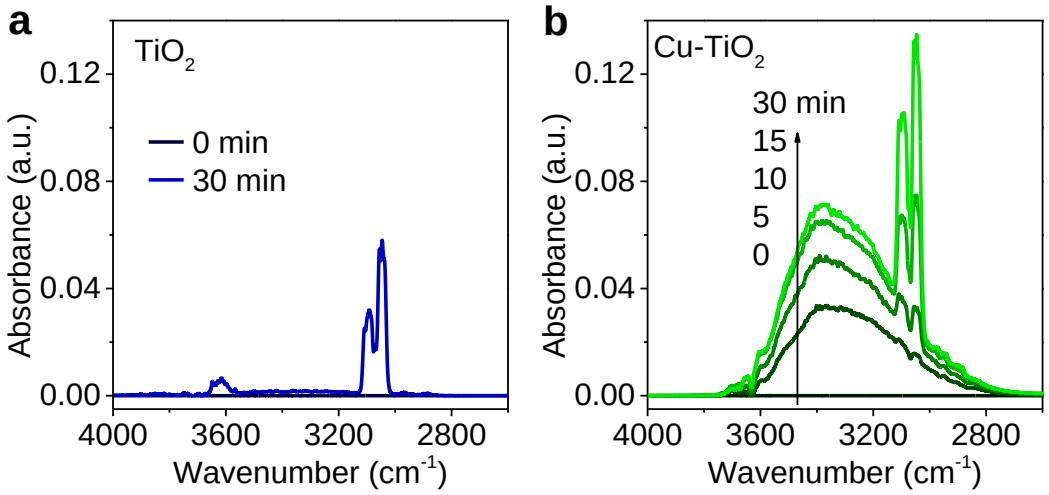

Figure S7. The *in situ* DRIFT characterizations for the absorption of benzene and moisture (H_2O) by TiO_2 (a) and Cu-TiO_2 (b).

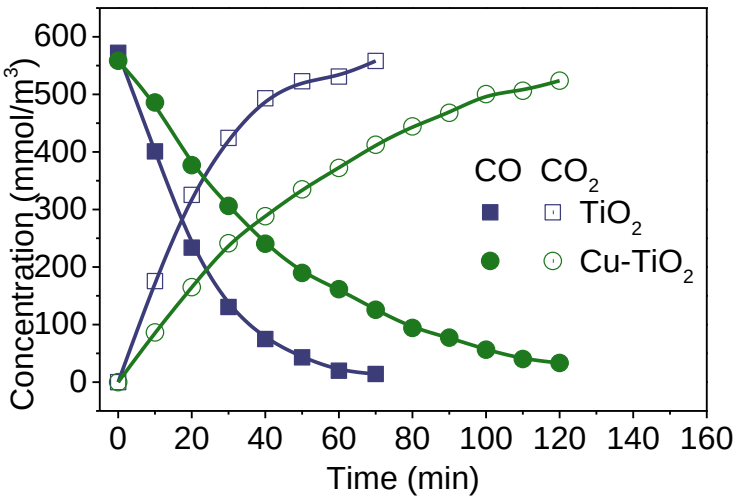

Figure S8. Photocatalytic oxidation behaviors of CO over TiO_2 and Cu-TiO_2 in a sealed system.

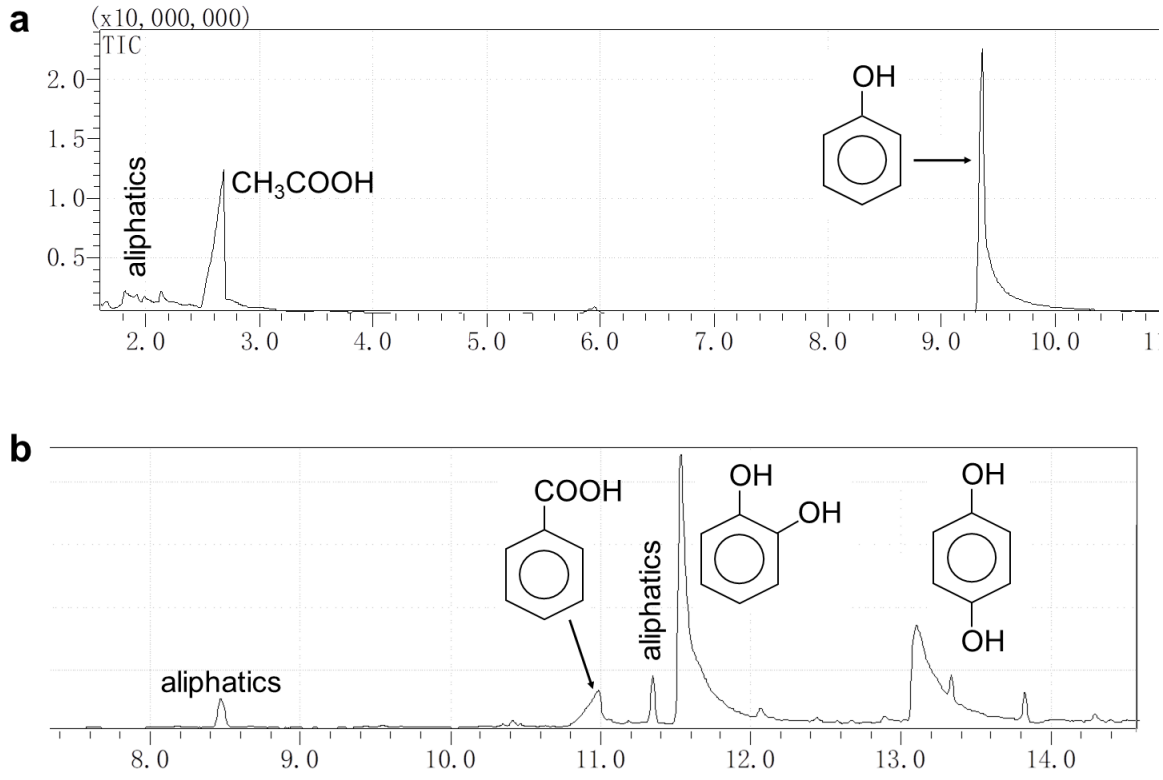

Figure S9. The intermediate produced during the degradation reaction (a, 30 min; b, 3 h) of benzene characterized by gas chromatography-mass spectrometry.

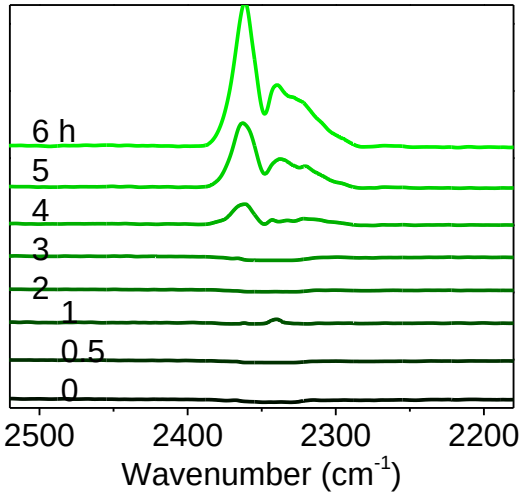

Figure S10. The *in situ* DRIFT analysis shows that the benzene can be eventually mineralized under the photocatalysis of Cu-TiO_2.

Computational Details

Density functional theory calculations are performed with projector augmented wave (PAW) method,[1] generalized gradient approximation (GGA) in the form of Perdew-Burke-Ernzerhof (PBE) for the exchange-correlation functional,[2, 3] and a plane-wave basis set with an energy cutoff of 400 eV, as implemented in VASP.[4, 5] The anatase TiO_2 (101) surface is modelled using a (2×2) supercell, four TiO_2 layers, and a vacuum layer of 15 Å. The surface Brillouin zone is sampled using a k-mesh of 2×3×1. During optimization, the bottom two TiO_2 layers are fixed at their bulk positions, while the rest atoms and adsorbates are freely relaxed until force acting on each atom converges below 0.05 eV/Å. The Hubbard-U correction with a U value of 7 eV is applied to the 3d electrons of Cu dopant to describe the on-site Coulomb interaction.[6] Van der Waals interaction is taken into account using the zero damping D3 method.[7] The free energy of solvated $^{\bullet}OH$ radical is 2.4 eV, which is taken from experiment and consistent with previous study.[8] The free energy of proton and electron pair is calculated according to the computational hydrogen electrode (CHE) model.[9]

Experimental procedure

Preparation of TiO_2 Materials. Cu-doped TiO_2 can be prepared by solvothermal method. Firstly, 0.1414 g $Cu(NO_3)_2 \cdot 3H_2O$ were dispersed into 20 mL tetrabutyl titanate by vigorously stirring at room temperature for 30 minutes. Then, 6.7 mL acetic acid were added into the dispersion. After stirring for 1 hour, the dispersion was transferred into a sealed 100-mL PTFE autoclave that was heated at 220 °C for 12 h. After reaction, the precipitate was washed with pure water and absolute ethanol for several times. After that, the product was dried under vacuum at 60 °C for 12 h. The TiO_2 was synthesized through the above procedure without addition of $Cu(NO_3)_2 \cdot 3H_2O$.

Material Characterization. The morphologies of samples were characterized by Field

Emission Scanning Electron Microscope (JSM-7900F). Powder X–ray diffraction (XRD) patterns were measured by a Bruker D8 Advanced diffractometer operating with a Cu *K*α X-ray source (λ=1.5405 Å). X-ray photoelectron spectroscopy (XPS) and ultraviolet photoelectron spectroscopy (UPS) measurements were carried out on an ThermoFisher EscaLab 250Xi emission using a monochromatic Al *K*α source (Ephoton = 1486.6 eV). Inductively coupled plasma-optical emission spectroscopy (ICP-OES) was carried out on Agilent ICP-OES730. UV-vis absorption spectra were recorded by performing a Shimadzu UV-3600 spectrometer. Steady-state photoluminescence (PL) spectra were obtained by a Hitachi F-7000 FL spectrophotometer. Fourier transform infrared (FTIR) spectra were collected by employing a Thermo Nicolet 380 infrared spectrophotometer with a KBr pellet technique. Transmission electron microscopy (TEM) investigations were taken with a JEOL JEM-2100 field emission electron microscope operated at 200 kV. The selected area electron diffraction (SAED) pattern of the samples was obtained by fast Fourier transform of the TEM image using Digital Micrograph software (Gatan).

Temperature-programmed desorption (TPD) of benzene measured by Gasmet DX4000. Sample powder (0.25 g) was pretreated in a quartz tube at 110 °C for 1 h under a high-pure N_2 flow, and then the system was cooled to 50 °C. For gaseous benzene adsorption, the sample was blown with 500 ppm benzene (in high-pure N_2 flow) for 1 h at 50 °C. After adsorption, the sample was purged with high-pure N_2 for 5 min and then benzene-TPD profile of the sample was recorded by increasing the temperature from 50 °C to 550 °C at a rate of 10 °C/min under high-pure N_2 flow.

In-situ diffuse reflectance infrared Fourier transform (DRIFT) spectra of benzene (and moisture) absorption were measured by performing a Bruker Tensor II spectrometer. Prior to operating the DRIFT, the catalyst in the sample chamber was purged by Ar gas flow (25 mL/min). After that, the

catalyst was heated at 110 °C for 1.5 h. After cooling down to 30 °C, gaseous benzene (and moisture) that carried by nitrogen gas was purged into the chamber for monitoring the absorption behaviors.

Measurements for photoelectrochemical generation and electrochemical determination of hydroxyl radicals were carried out in a standard three-electrode system, in which a carbon cloth was used as counter electrode and an Ag/AgCl electrode was used the reference. The photo-induced anodic behaviors and the resulted cathodic reaction can be monitored by measuring the disk and ring currents of a rotating ring disk electrode (RRDE) working electrode that connected to a CHI 760D electrochemical workstation. To avoid the occurrence of oxygen reduction, the electrolyte (1 M Na_2SO_4) was bubbled with argon. The irradiation for the (photo)-electrochemical measurements was provided by a 500-W Hg-lamp (PerfectLight, CHF-XM-500). To prepare a working electrode, the dispersion was formed by mixing 20 mg catalysts (TiO_2 or Cu-TiO_2), 1 mL ethanol, and 200 μL Nafion under sonication. Subsequently, 5 μL of catalyst dispersion was drop-casted onto a precleaned glassy carbon ring electrode and dried naturally.

Photocatalysis. The closed benzene photodegradation reaction was carried out in a self-made 310 mL annular quartz reactor with Hg-lamp (PHILIPS, TUV, 15 W/G15) inside, two sampling mouths and a magnetic stirring device. The Hg-lamp was coated with catalyst slurry (50 mg catalyst and 0.5 mL water was mixed with stirring for 5 min), and dried naturally. After the loading of catalyst onto the lamp, 2 μL benzene was injected followed with stirring in dark for 30 min to achieve adsorption-desorption equilibrium. Then Hg-lamp was turned on, and the concentrations of benzene, CO and CO_2 during the photocatalytic degradation process were monitored by gas chromatography (equipped with an FID detector).

In-situ diffuse reflectance infrared Fourier transform spectroscopy (DRIFT) was conducted to

explores the degradation pathways of benzene. Prior to performing the DRIFT, the catalyst in the sample chamber was purged by Ar gas flow (25 mL/min). After that, the catalyst was heated at 110 °C for 1.5 h. After cooling down to 40 °C, 2 μL benzene was dropped into the reaction chamber. After sealing the chamber, Hg-lamp was turned on for investigation the behaviors of benzene degradation.

The intermediates formed during the benzene degradation was identified by gas chromatography-mass spectrometer (Shimadzu GCMS-QP2010 Ultra). The intermediates were collected by washing the reactor with methanol. The column temperature program of gas chromatography was set as follows: the initial temperature of 40 °C stayed for 1 min, then heated to 200 °C with a heating rate of 5 °C/min, then 10 °C/min to 250 °C. The injector temperature was 250 °C and the ionization temperature was 200 °C.

To meet the requirement of practical applications, a continuous air-flow photocatalytic system equipped with a gas mixer was fabricated. The catalyst slurry was formed by mixing 300 mg catalyst, 300 mg polyethylene glycol (20 000) and 2 mL H_2O, and then shook in a 3D powder mixer for 12 h. After the slurry coated on a 320-W UV lamp and dried naturally, the lamp was annealed at 400 °C for sintering. Then the lamp coated with photocatalyst was placed into the reactor. The reaction was performed by inletting the air flow (containing various concentrations of benzene) through the reaction chamber at a rate of 100 L/min. The required moisture was provided by injecting water (0.5 mL/min) into a steam generator that connected with the photocatalytic reactor in series. The concentrations of benzene in the air flow before and after photocatalytic treatment were monitored by a gas chromatography (FID detector). The degradation efficiency of benzene can be calculated by: $(1 - C/C_0) \times 100\%$, where C_0 is the inlet concentration and C was the treated concentration.

References

1. G. Kresse and D. Joubert, *Phys. Rev. B*, 1999, **59**, 1758-1775.

2. J. P. Perdew, K. Burke and M. Ernzerhof, *Phys. Rev. Lett.*, 1996, **77**, 3865-3868.

3. B. Hammer, L. B. Hansen and J. K. Nørskov, *Phys. Rev. B*, 1999, **59**, 7413-7421.

4. G. Kresse and J. Furthmüller, *Comput. Mater. Sci.*, 1996, **6**, 15-50.

5. G. Kresse and J. Furthmüller, *Phys. Rev. B*, 1996, **54**, 11169-11186.

6. Y. Maimaiti, M. Nolan and S. D. Elliott, *Phys. Chem. Chem. Phys.*, 2014, **16**, 3036-3046.

7. S. Grimme, J. Antony, S. Ehrlich and H. Krieg, *J. Chem. Phys.*, 2010, **132**, 154104.

8. S. Siahrostami, G.-L. Li, V. Viswanathan and J. K. Nørskov, *J. Phys. Chem. Lett.*, 2017, **8**, 1157-1160.

9. J. K. Nørskov, J. Rossmeisl, A. Logadottir, L. Lindqvist, J. R. Kitchin, T. Bligaard and H. Jonsson, *J. Phys. Chem. B*, 2004, **108**, 17886-17892.